Termination-Dependence of Resistive Switching in $SrTiO_3$-based Valence Change Memory

M. Mladenović, M. Kaniselvan, C. Weilenmann, A. Emboras, and M. Luisier
*Integrated Systems Laboratory, ETH Zürich, Gloriastrasse 35, 8092, Zürich, Switzerland
e-mail: mmladenovic@iis.ee.ethz.ch

Valence change memories (VCMs) are resistive switching devices that have been recently proposed as solid-state synapses in neuromorphic computing applications. VCM devices typically achieve their switchable resistances through a reversible filamentary dielectric breakdown within an oxide layer [1] (**Fig. 1(a)**, left). Once a transition to the low resistance state (LRS) is complete, the resulting filament of conductive oxygen vacancies leads to linear current-voltage (I-V) characteristics (**Fig. 1(b)**, left). VCM based on $SrTiO_3$, however, can also exhibit distinctively nonlinear LRS I-V characteristics (**Fig. 1(a)**, right) that have been attributed to the modulation of the Schottky barrier height at the high-work-function contact through an accumulation of oxygen vacancies at that location [2] (**Fig. 1(b)**, right). Previous reports suggest that a conductive filament might also be present in these devices [3], potentially resulting in a combination of both filamentary and interface-type switching. Using *ab-initio* methods, we reveal here that the switching mechanism of these devices may be strongly influenced by the $SrTiO_3$ edge termination.

We consider a Pt-$SrTiO_3$-Ti stack (**Fig. 1(c)**) with two different terminations of crystalline $SrTiO_3$: SrO and TiO_2, as shown in **Fig. 2(a)**. The same termination is used at both interfaces. Optimized atomic device structures are obtained from density functional theory calculations, while the electric currents are calculated with a quantum transport solver [4]. We investigate the effect of oxygen vacancies on the transport properties of $SrTiO_3$ devices by constructing two distinct models, one with a uniform distribution of the vacancies (**Fig. 2(b)**, top) and one with vacancies accumulated at the Pt electrode (**Fig. 2(b)**, bottom), representing idealized filamentary- and interface-type LRS states, respectively. The resulting I-V characteristics of both distributions applied to the SrO-/TiO_2-terminated devices are shown in the left/right subplots of **Fig. 2(c)**. In the case of the SrO-terminated device, the uniform distribution exhibits a higher current, indicating a filamentary-type conduction mechanism dominated by hopping through the oxide. In contrast, the device with the TiO_2-terminated surface has a higher current when vacancies are accumulated at the Pt-end, indicating that transport here is limited by the interface.

We analyze the transport mechanism further in **Fig. 3(a)** by plotting the Local Density-of-States (LDOS) and energy-resolved currents for the four cases in **Fig. 2(c)**. The LDOS and current of the SrO-terminated cell indicate that the higher current with uniformly-distributed vacancies (**Fig. 3(a)**, top left) originates from transport through defect states created in the band gap of the oxide. Accumulation of vacancies at the Pt end, meanwhile, still leaves a high tunneling gap which impedes current flow, as illustrated in **Fig. 3(b)**, top right.

The LDOS and current for the TiO_2-termination (**Fig. 3(a)**, bottom) present a different picture in which current is primarily injected into the conduction band from the Ti-contact. The electrons encounter a Schottky barrier at the Pt-end, whose height can be modulated by the accumulation of the oxygen vacancies, as can be seen in **Fig. 3(a) and 3(b)**, bottom.

Our results indicate the possibility of interface-engineering $SrTiO_3$-based VCM cells to influence the dominant conduction mechanism.

References

[1] W. A. Hubbard, et al, *Adv. Funct. Mater.* **32**, 2102313 (2022).
[2] D. Cooper, et al, *Adv. Mater.* **29**, 1700212 (2017).
[3] S. Stille, et al, *Appl. Phys. Lett.* **100**, 223503 (2012).
[4] M. Luisier, et al, *Phys. Rev. B* **74**, 205323 (2006).

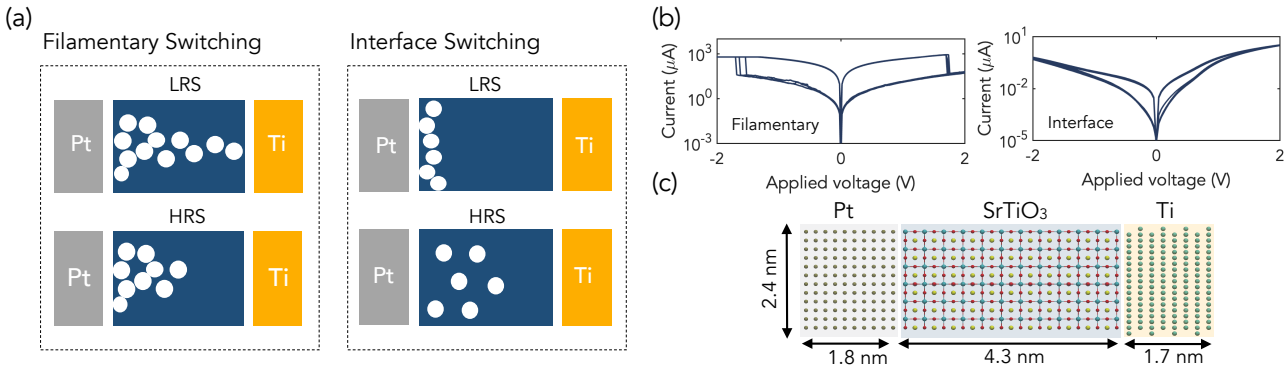

Fig. 1. (a) Illustrations of the low (top) and high resistance state (bottom) corresponding to the interface (left) and filamentary switching (right) of metal-oxide-metal memory cells. White circles refer to oxygen vacancies and the blue region represents the switching material. (b) Experimentally measured I-V characteristics of interface (left) and filamentary switching (right) of Pt-$SrTiO_3$-Ti memory cells. (c) Atomic structure of the simulated Pt-$SrTiO_3$-Ti stack. The out of plane direction measures 2 nm.

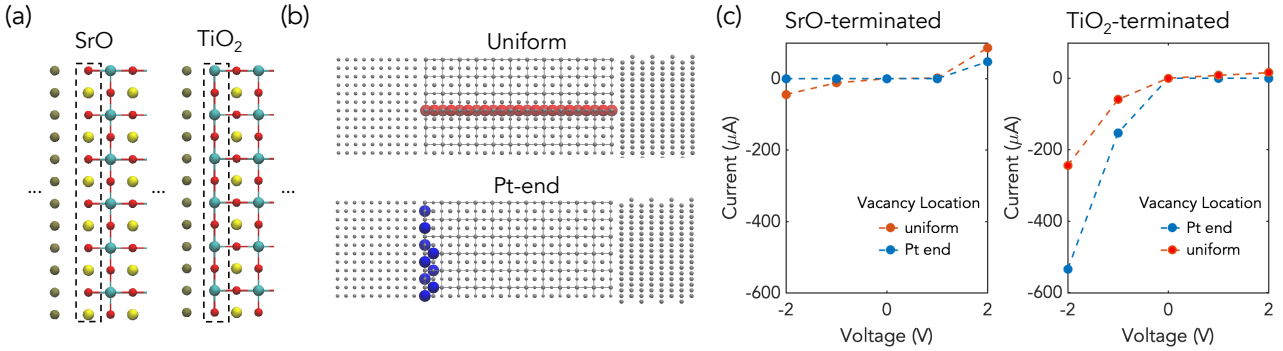

Fig. 2. (a) Atomic structure of a SrO- (left) and a TiO_2-terminated (right) Pt-$SrTiO_3$-Ti stack. (b) Uniform distribution of vacancies (top) and accumulation of vacancies at the Pt electrode (bottom). (c) I-V characteristics of the SrO- (left) and TiO_2-terminated (right) devices for the two vacancy distributions shown in (b).

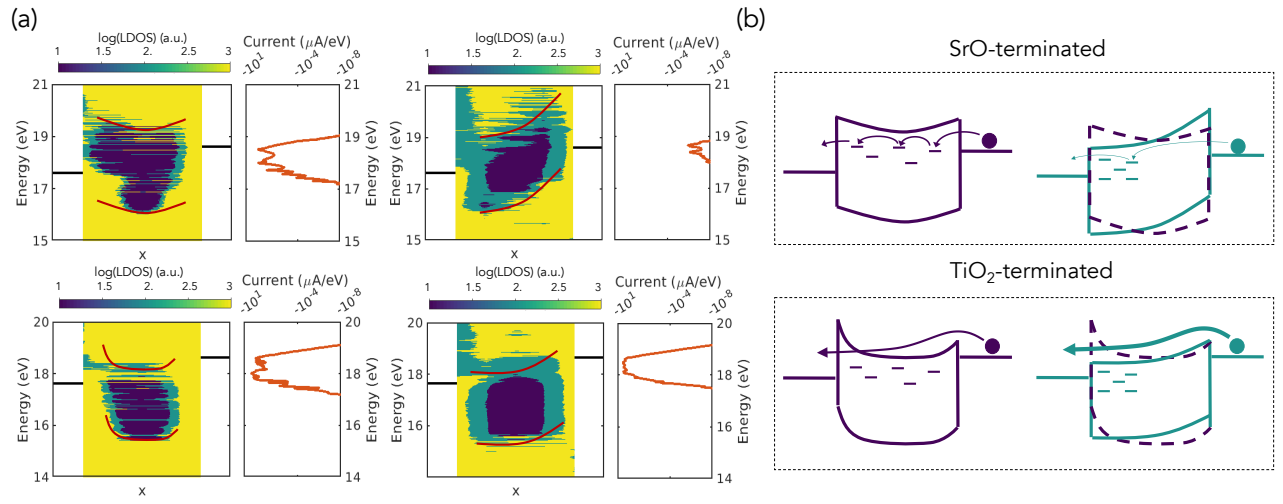

Fig. 3. (a) Local Density-of-States and energy-resolved current of Pt-$SrTiO_3$-Ti stacks with uniformly distributed vacancies (left) and vacancies accumulated at the Pt electrode (right) for SrO (top) and TiO_2 (bottom) terminations, under an applied bias of -1V. The black horizontal lines indicate the Fermi levels in the contacts, while the red lines are band edges visually approximated from the DOS. (b) Schematic view of the band diagrams and transport regimes corresponding to the four cases depicted in (a). The dashed lines on the right-side diagrams correspond to the band edges of the left-side diagrams for comparison.